Antiferromagnetism in the kagome-lattice compound α-$Cu_3Mg(OH)_6Br_2$

Yuan Wei,[1,2] Zili Feng,[1,2] Clarina dela Cruz,[3] Wei Yi,[4] Zi Yang Meng,[1,5,6,7] Jia-Wei Mei,[8] Youguo Shi,[1,9,6,*] and Shiliang Li[1,2,6,†]

[1]*Beijing National Laboratory for Condensed Matter Physics, Institute of Physics, Chinese Academy of Sciences, Beijing 100190, China*
[2]*School of Physical Sciences, University of Chinese Academy of Sciences, Beijing 100190, China*
[3]*Neutron Scattering Division, Neutron Sciences Directorate, Oak Ridge National Laboratory, Oak Ridge, Tennessee 37831, USA*
[4]*International Center for Materials Nanoarchitectonics, National Institute for Materials Science, 1-1 Namiki, Tsukuba, Ibaraki 305-0044, Japan*
[5]*CAS Center of Excellence in Topological Quantum Computation and School of Physical Sciences, University of Chinese Academy of Sciences, Beijing 100190, China*
[6]*Songshan Lake Materials Laboratory, Dongguan, Guangdong 523808, China*
[7]*Department of Physics, The University of Hong Kong, China*
[8]*Shenzhen Institute for Quantum Science and Engineering, and Department of Physics, Southern University of Science and Technology, Shenzhen 518055, China*
[9]*Center of Materials Science and Optoelectronics Engineering, University of Chinese Academy of Sciences, Beijing 100049, China*

(Received 1 May 2019; revised manuscript received 20 July 2019; published 16 October 2019)

The antiferromagnetism in α-$Cu_3Mg(OH)_6Br_2$ was studied by magnetic-susceptibility, specific-heat, and neutron-diffraction measurements. The crystal structure consists of Cu^{2+} kagome layers with Mg^{2+} ions occupying the centers of the hexagons, separated by Br^{1-} ions. The magnetic system orders antiferromagnetically at 5.4 K with the magnetic moments aligned ferromagnetically within the kagome planes. The ordered moment is $0.94\mu_B$, suggesting little quantum and geometrical fluctuations. By comparing the magnetic and specific-heat properties with those of the haydeeite, we suggest that α-$Cu_3Mg(OH)_6Br_2$ may be described by the two-dimensional spin-1/2 Heisenberg kagome model and is in the region of the ferromagnetic-order side of the phase diagram.

DOI: 10.1103/PhysRevB.100.155129

I. INTRODUCTION

The two-dimensional (2D) spin-1/2 kagome model has been a subject of intense theoretical study due to its rich ground states [1–16]. For example, the $S = 1/2$ Heisenberg antiferromagnetic kagome model (AFKM) can give rise to ferromagnetic (FM) order, different types of antiferromagnetic (AFM) orders, and quantum spin liquids (QSLs) [7]. The AFKM may be realized in many minerals of the atacamite group with the molecular formula $Cu_3T(OH)_6X_2$, where T and X are the $3d$ nonmagnetic transition metal (Zn,Mg) and the halogen elements (F,Cl,Br), respectively. The most well-known material is the herbertsmithite $Cu_3Zn(OH)_6Cl_2$, which shows no magnetic order down to at least 30 mK and is suggested to be a QSL [17–24]. The structure of γ-$Cu_3Mg(OH)_6Cl_2$ is very similar to that of the herbertsmithite, and it may also have a QSL state [25]. Recently, new materials $Cu_3Zn(OH)_6FBr$ and $Cu_3Zn(OH)_6FCl$ with similar structure have been successfully synthesized and shown possibly to contain the gapped Z_2 QSL ground states [26–29].

In the above materials, the kagome layers formed by Cu^{2+} ions are separated by nonmagnetic Zn or Mg ions, which may be treated as a diamagnetic dilution of the three-dimensional (3D) pyrochlore-like lattice. These nonmagnetic ions can also occupy the center of the hexagons in the kagome layers, as found in kapellasite, α-$Cu_3Zn(OH)_6Cl_2$ [30], and haydeeite, α-$Cu_3Mg(OH)_6Cl_2$ [31]. In this structure, the coupling between the kagome layers is through the weak interlayer O-H-Cl bonding, which should result in highly 2D magnetic properties. It had been suggested that the kapellasite may be a gapless spin liquid or noncoplanar coboc2-type AF order [3,32], but later measurements found strong Cu/Zn site mixing that makes the AFKM inappropriate [33]. The haydeeite is a rare example of FM order for kagome magnets with T_c at 4.2 K [34]. Measurements on single-crystal haydeeite further revealed strong anisotropic behaviors between in-plane and out-of-plane magnetic properties [35]. Although the magnetic structure has not been unambiguously solved, the ordered moment is less than $0.2\mu_B$, suggesting strong quantum fluctuations. Therefore, the haydeeite may be in close proximity to the quantum phase transition between the Heisenberg kagome FM order and the Heisenberg cuboc2 AF order [34].

The idea for the compound $Cu_3Mg(OH)_6Br_2$ comes from the substitution of interlayer Cu^{2+} in the barlowite $Cu_4(OH)_6FBr$, which has perfect Cu^{2+} kagome layers with Cu^{2+} ions between them and is antiferromagnetically ordered at about 15 K [36–40]. It has been theoretically suggested that Zn^{2+} or Mg^{2+} ions can replace the interlayer Cu^{2+} in barlowite and thus dilute the AF order to give rise to a QSL state as in herbertsmithite [41,42]. While this proposal has

*ygshi@iphy.ac.cn
†slli@iphy.ac.cn

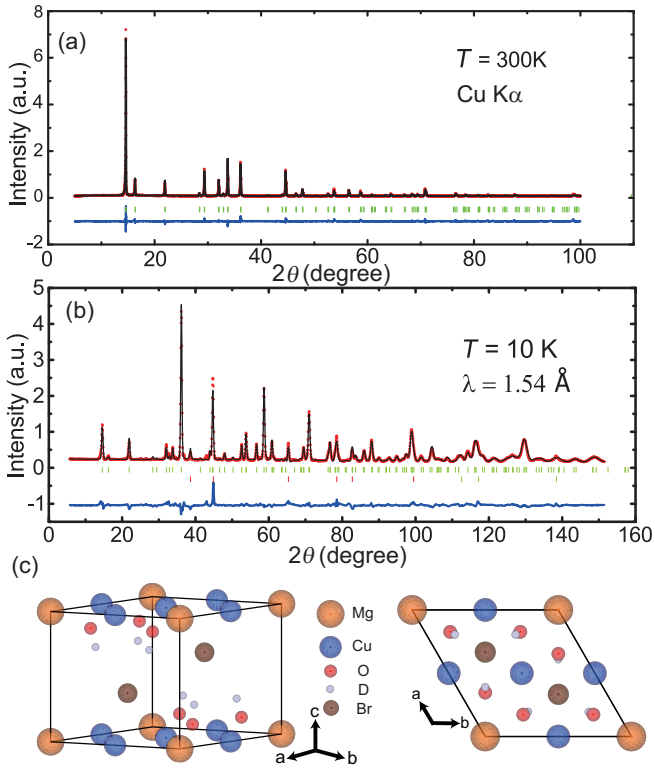

FIG. 1. (a) and (b) X-ray and neutron powder diffraction intensities of α-$Cu_3Mg(OD)_6Br_2$ (red dots) at 300 and 10 K, respectively. The calculated intensities are shown by the black lines. Short vertical green lines represent calculated Bragg peak positions. Vertical red lines represent Al peaks, which only exist in the neutron diffraction experiment due to the use of an Al can. The blue lines show the differences between measured and calculated intensities. The weighted profile R-factor (R_{wp}) at 300 and 10 K are 7.262% and 7.66%, respectively. Impurities are found in the neutron-scattering sample. These chemical impurities only exist in the deuterated sample. (c) Nuclear structure of α-$Cu_3Mg(OD)_6Br_2$ (3D and top views).

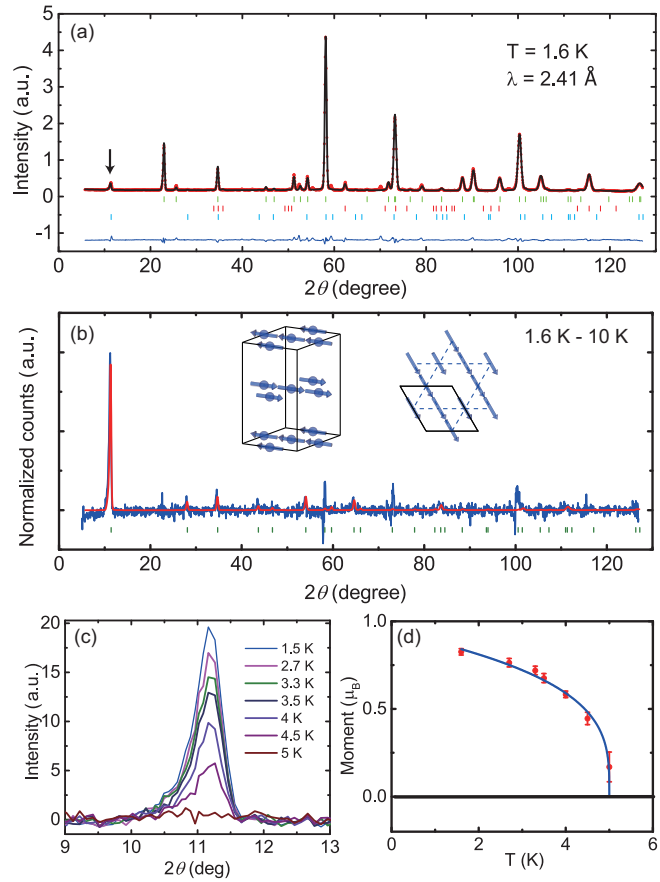

FIG. 2. (a) Neutron powder diffraction intensities of α-$Cu_3Mg(OD)_6Br_2$ (red dots) at 1.6 K. The lines represent the same meanings as those in Fig. 1(a). The vertical blue lines represent magnetic peaks. The arrow shows the new peak that appeared at this temperature. The weighted profile R-factor (R_{wp}) is 14.1%. (b) The difference (blue lines) between the intensities at 1.6 and 10 K for α-$Cu_3Mg(OD)_6Br_2$. The red lines represent the calculated intensities for the magnetic peaks. The vertical green lines represent magnetic peaks. The inset shows the magnetic structure. (c) The temperature dependence of the magnetic peak at (0, 0, 0.5). (d) The temperature dependence of the moment. The error bars are from the refinements. The solid line is the fitted result as described in the main text with T_N fixed at 5 K, which is slightly different from that determined from the thermodynamic measurements as shown later, most likely due to the sample environment used in the neutron-diffraction experiment.

been shown to succeed in $Cu_3Zn(OH)_6FBr$ [26–28,39,43], no Mg-substituted barlowite has been reported. In this paper, we follow the same route in synthesizing the Zn-substituted barlowite to grow Mg-substituted barlowite. However, the final product is $Cu_3Mg(OH)_6Br_2$ because MgF_2 cannot be dissolved in water. Since it has the same crystal structure as kapellasite and haydeeite, we label it as α-$Cu_3Mg(OH)_6Br_2$. The system orders antiferromagnetically at about 5.4 K but the configuration of the moments within the kagome plane is FM with the ordered moment of $0.94\mu_B$. Our results suggest that α-$Cu_3Mg(OH)_6Br_2$ is in the FM region of the phase diagram in the 2D Heisenberg kagome model.

II. EXPERIMENTS

α-$Cu_3Mg(OH)_6Br_2$ was synthesized by the hydrothermal method as described previously [26,39]. The mixture of 1.5-mmol $Cu_2(OH)_2CO_3$ and 6-mmol $MgBr_2 \cdot 6H_2O$ was sealed in a 50-mL reaction vessel with 25-mL water, which was slowly heated to 200 °C and kept for 12 h. The polycrystalline samples were obtained by washing the production with the deionized water. To produce deuterated samples, $Cu_2(OD)_2CO_3$ and heavy water were used in the above process. The Mg content is determined by the inductively coupled plasma mass spectrometer. The magnetic susceptibility and heat capacity were measured by MPMS and PPMS (Quantum Design), respectively. The nuclear structure at room temperature was determined by powder x-ray diffraction (XRD) on a Rigaku ultima IV X ray Diffractometer. The magnetic and nuclear structures at low temperatures were determined by neutron diffraction experiments performed on the HB-2A diffractometer at HFIR, USA, with wavelengths of both 2.4103 and 1.5395 Å. The nuclear and magnetic structures are refined by the FULLPROF program [44].

TABLE I. Nuclear structure parameters of α-$Cu_3Mg(OD)_6Br_2$ at 10 K. $P\bar{3}m1$ (no. 164): $a = b = 6.293\,14(20)$ Å, $c = 6.106\,37(25)$Å, $\alpha = \beta = 90^\circ$, and $\gamma = 120^\circ$.

	Site	x	y	z	B (Å^2)
Mg	1a	0.00000	0.00000	0.00000	0.281(406)
Cu	3e	0.50000	0.00000	0.00000	0.131(131)
Br	2d	0.33333	0.66667	0.63819(90)	0.117(155)
O	6i	0.82592(32)	0.17418(32)	−0.14100(64)	0.511(120)
D	6i	0.19300(41)	0.80700(41)	0.28666(98)	0.398(140)

III. RESULTS AND DISCUSSIONS

Figures 1(a) and 1(b) show the powder diffraction results at 300 and 10 K obtained by the XRD and neutron diffraction techniques, respectively. Refinements on these data give the same hexagonal nuclear structure with the space group $P\bar{3}m1$, which suggests that there is no structural transition. Detailed refinement results at 10 K are shown in Table I. Since the coherent neutron scattering lengths of Cu and Mg are very different, their occupancies can be reliably refined. The values are 1.000(20) and 1.073(60) for Cu and Mg, respectively, if only one element is put onto 3e and 1a sites. On the other hand, one can only obtain a very small negative occupancy value for either Cu at 1a or Mg at 3e site. Therefore, we conclude that there is no site mixing of Cu and Mg ions. Figure 1(c) gives the nuclear structure [45]. The Cu^{2+} ions form kagome planes, which are separated by Br^{1-} ions. The Mg^{2+} ions sit at the centers of the hexagons within the Cu^{2+} kagome planes.

At 1.6 K the system becomes magnetically ordered, as shown by the new peak in Fig. 2(a). The subtraction between the 1.6 and 10 K data shows several magnetic peaks, as shown in Fig. 2(b). The k-search method based on the first three, four, and five magnetic peaks all yields a propagation vector $k = (0, 0, 0.5)$. The SARAH program [46,47] was used to check the possible structures from the results of a representational analysis based on the nuclear space group and magnetic propagation vector k. There are three irreducible representations (IRs), Γ_1, Γ_3, and Γ_5, which give the magnetic space groups as $P\bar{3}m1$, $P\bar{3}m'1$, and $P1$, respectively. These three IRs have 10 basis vectors (BVs) [45], where ψ_6 gives the best-fitting results. The inset of Fig. 2(b) shows the magnetic structure. The moments at Cu^{2+} positions are confined within the kagome planes and ferromagnetically aligned along the b-axis. Along the c-axis, the moments are aligned antiferromagnetically.

Figure 2(c) shows the temperature dependence of the magnetic peak at (0, 0, 0.5) in the nuclear structural notation. Figure 2(d) shows the temperature dependence of the refined moment, which can be fitted by $M_0(1 - T/T_N)^\beta$. The values of M_0 and β are $0.94 \pm 0.03\mu_B$ and (0.29 ± 0.03), respectively. The ordered moment M_0 at 0 K is consistent with the ordered moment gS for an $S = 1/2$ system with $g = 2$.

Figure 3(a) gives the temperature dependence of the M/H, which clearly shows an AF phase transition at $T_N = 5.54$ K.

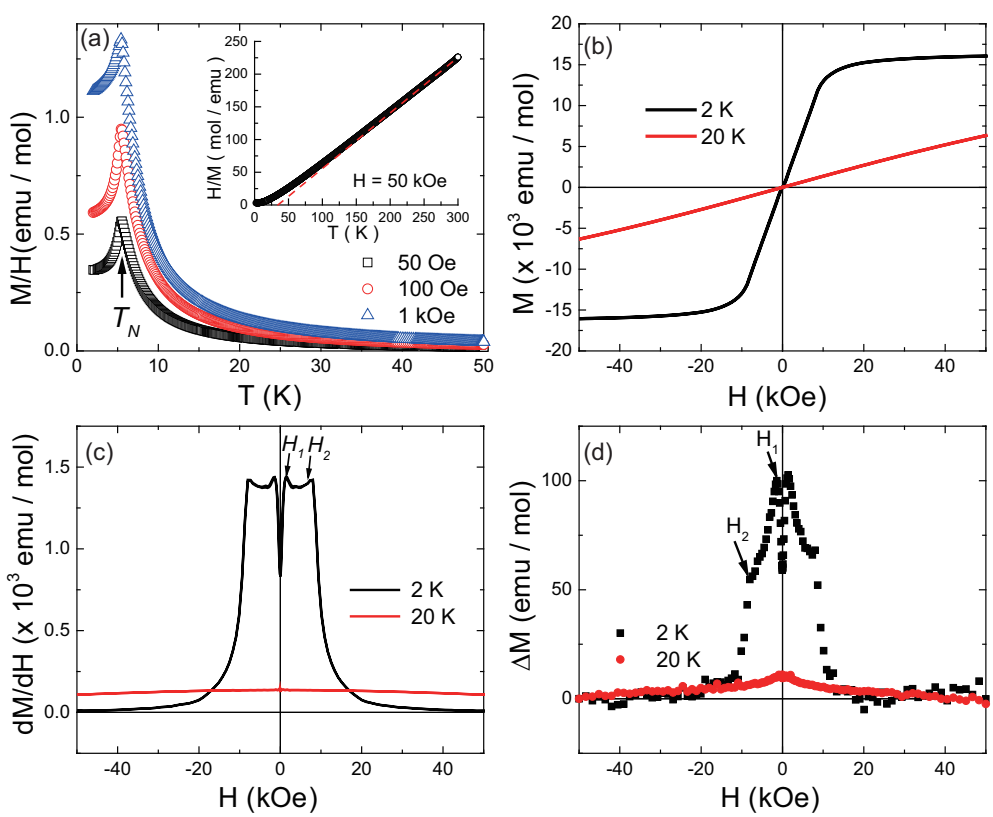

FIG. 3. (a) Temperature dependence of the M/H at 50 Oe, 100 Oe, and 1 kOe. The arrow indicates the AF phase transition temperature. The inset shows the temperature dependence of H/M at 50 kOe. The dashed line is the linear fit to the high-temperature data. (b) M-H loops at 2 and 20 K. (c) dM/dH at 2 and 20 K. (d) The difference of M between increasing and decreasing fields at 2 and 20 K.

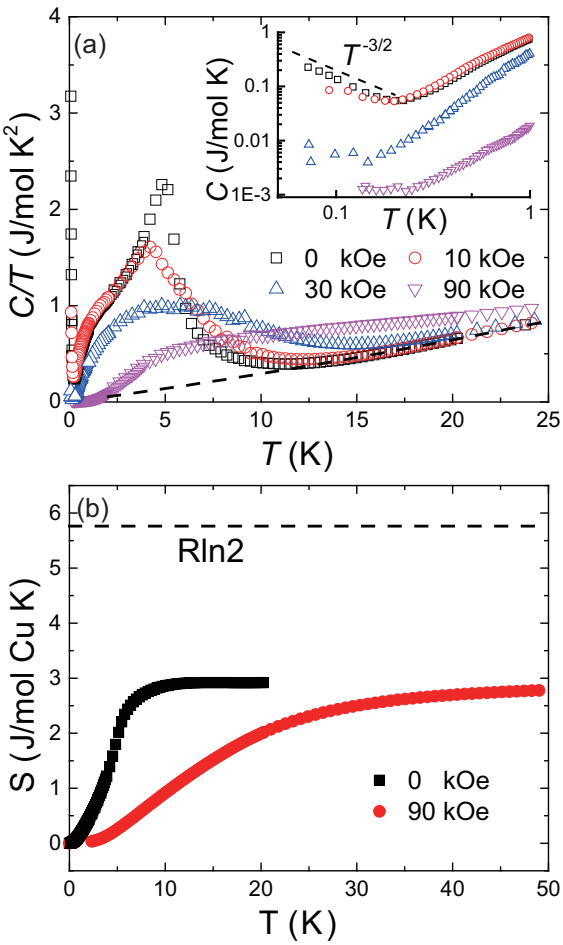

FIG. 4. (a) Temperature dependence of C/T at several fields. The black dashed line is the fitted result for the phonon contribution as discussed in the main text. The inset shows the specific heat C below 1 K. (b) Magnetic entropy associated with the magnetic transition at 0 and 90 kOe.

No significant difference is found between the field-cooled and zero-field-cooled processes. Above T_N, M/H still depends strongly on the magnetic field, which suggests the presence of 2D spin fluctuations. The inset shows the temperature dependence of H/M at 50 kOe, which is roughly equivalent to the inverse of the magnetic susceptibility. The fitting at high temperatures gives a Curie temperature θ of about 34 K and an effective moment of $1.77\mu_B$, which is close to the value for $S = 1/2$ with $g = 2$, i.e., $g\sqrt{S(S+1)} = 1.732\mu_B$. Figure 3(b) shows the field dependence of the magnetization M. At 2 K, M becomes saturated above 20 kOe with the saturated moment of $0.95\mu_B$, which also suggests that the system is $S = 1/2$. By taking the first derivative, two features can be seen at $H_1 \approx 1.4$ kOe and $H_2 \approx 8$ kOe as shown in Fig. 3(c). The value of H_1 is similar to the saturated field for the field parallel to the kagome planes in haydeeite [35], which suggests that the easy-axis is within the kagome plane. These two characteristic fields can also be seen by the hysteresis behavior as shown in Fig. 3(d).

Figure 4(a) shows the specific heat of α-$Cu_3Mg(OH)_6Br_2$ at several magnetic fields. The AF transition results in a large peak, which becomes a broad hump above 3 T due to the suppression of the transition. The background of the specific heat can be estimated by fitting the data from 15 to 30 K with $C = \alpha T^2 + \beta T^3$ as shown by the dashed line in Fig. 4(a). The fitted values for α and β are 0.0265 J/mol K^3 and 2.86×10^{-4} J/mol K^4, respectively, similar to those in barlowite [36]. The cubic and square terms are from the contributions from phonons and 2D magnetic fluctuations, respectively. Figure 4(b) shows the temperature dependence of the entropy released associated with the magnetic transition, which is obtained by the integration of C/T after subtracting the background as described above. The value of ΔS_{AF} at high temperature is about 3 J/mol Cu K, which is just about half of $R\ln 2$. This is the typical behavior for quasi-2D spin systems, where spin correlations are formed well above T_N, as shown by the large value of α and θ in fitting the specific heat and magnetic susceptibility above T_N, respectively. It suggests that the magnetic couplings within the kagome planes should be much larger than that along the c-axis.

Interestingly, there is an upturn of C below 0.2 K as shown in the inset of Fig. 4(a), which can be fitted as $C \propto T^{-3/2}$. This kind of temperature dependence suggests that the upturn is not from the nuclear Schottky anomaly or magnetic impurities. Moreover, the specific heat should move to higher temperatures under fields if it comes from the nuclear Schottky anomaly or magnetic impurities. Instead, it is suppressed at 30 kOe and thus should be related to the intrinsic kagome system before the spins are fully polarized by the field. The entropy between 0.07 and 0.2 K is about 0.12 J/mol K. It is not clear what the origin of this upturn is, but it is rather surprising since the system shows no exotic properties from other measurements.

Our results suggest that α-$Cu_3Mg(OH)_6Br_2$ is another example for 2D Heisenberg kagome ferromagnetism. The antiferromagnetic alignment along the c-axis is due to the small interplane antiferromagnetic coupling. According to the 2D Heisenberg kagome model [6,34], the magnetic interactions within a kagome plane mainly include nearest J_1, next-nearest J_2, next-next-nearest J_3, and J_3'. For a ferromagnetic $J_1 < 0$, the system will show ferromagnetic order as far as J_2, J_3, and J_3' are negative or their absolute values are smaller than $|J_1|$. For haydeeite, it has been shown that its magnetic ground states may sit near the boundary between the FM and cuboc2 type noncoplanar AFM parts in the phase diagram since its ordered moment is just $0.2\mu_B$ due to strong quantum fluctuations [34]. In our case, the Curie-Weiss temperature from the magnetic-susceptibility measurement is 34 K, which is slightly larger than that in haydeeite (28 K) [34]. Considering that they have the same nuclear and in-plane magnetic structures, it is reasonable to conclude that, for α-$Cu_3Mg(OH)_6Br_2$, the dominated magnetic interaction is also the ferromagnetic J_1. Because the ordered moment of our sample is $0.94\mu_B$, the effect of quantum fluctuations should be much weaker. Therefore, α-$Cu_3Mg(OH)_6Br_2$ is most likely in the FM part that is away from the boundary. It is also worth noting that while there are diluting effects of Mg on Cu sites for haydeeite, our sample shows no site mixing between Mg and Cu. While the large ordered moment makes α-$Cu_3Mg(OH)_6Br_2$ less interesting due to the lack of frustration effects, it is worth noting that it may be another platform to study the topological bands in the kagome ferromagnet as observed in Cu[1,3-benzenedicarboxylate(bdc)] [48].

IV. CONCLUSIONS

Our systematic studies on the magnetism in α-$Cu_3Mg(OH)_6Br_2$ demonstrate that it orders antiferromagnetically below 5.54 K but the moments are aligned ferromagnetically within the kagome planes. The FM state of the kagome planes can be achieved easily by applying a weak magnetic field, and its fluctuations survive above T_N. Our results suggest that α-$Cu_3Mg(OH)_6Br_2$ is in the FM part in the phase diagram of the 2D Heisenberg kagome model.

ACKNOWLEDGMENTS

This work is supported by The National Key Research and Development Program of China (Grants No. 2017YFA0302900, No. 2016YFA0300502, and No. 2016YFA0300604), the National Natural Science Foundation of China (Grants No. 11874401, No. 11674406, No. 11574359, No. 11674370, and No. 11774399), the Strategic Priority Research Program(B) of the Chinese Academy of Sciences (Grants No. XDB25000000, No. XDB07020000, and No. XDB28000000), Beijing Natural Science Foundation (Grant No. Z180008), Guangdong Introducing Innovative and Entrepreneurial Teams (Grant No. 2017ZT07C062), and the National Thousand-Young Talents Program of China. Research conducted at ORNL's High Flux Isotope Reactor was sponsored by the Scientific User Facilities Division, Office of Basic Energy Sciences, U.S. Department of Energy.

Y.W. and Z.F. contributed equally to this work.

[1] S. Sachdev, Phys. Rev. B **45**, 12377 (1992).
[2] H. C. Jiang, Z. Y. Weng, and D. N. Sheng, Phys. Rev. Lett. **101**, 117203 (2008).
[3] O. Janson, J. Richter, and H. Rosner, Phys. Rev. Lett. **101**, 106403 (2008).
[4] S. Yan, D. A. Huse, and S. R. White, Science **332**, 1173 (2011).
[5] H.-C. Jiang, Z. Wang, and L. Balents, Nat. Phys. **8**, 902 (2012).
[6] L. Messio, C. Lhuillier, and G. Misguich, Phys. Rev. B **83**, 184401 (2011).
[7] L. Messio, B. Bernu, and C. Lhuillier, Phys. Rev. Lett. **108**, 207204 (2012).
[8] M. Punk, D. Chowdhury, and S. Sachdev, Nat. Phys. **10**, 289 (2014).
[9] S. Bieri, L. Messio, B. Bernu, and C. Lhuillier, Phys. Rev. B **92**, 060407(R) (2015).
[10] Y. Iqbal, H. O. Jeschke, J. Reuther, R. Valentí, I. I. Mazin, M. Greiter, and R. Thomale, Phys. Rev. B **92**, 220404(R) (2015).
[11] K. Kumar, K. Sun, and E. Fradkin, Phys. Rev. B **92**, 094433 (2015).
[12] S.-S. Gong, W. Zhu, K. Yang, O. A. Starykh, D. N. Sheng, and L. Balents, Phys. Rev. B **94**, 035154 (2016).
[13] H. J. Liao, Z. Y. Xie, J. Chen, Z. Y. Liu, H. D. Xie, R. Z. Huang, B. Normand, and T. Xiang, Phys. Rev. Lett. **118**, 137202 (2017).
[14] J.-W. Mei, J.-Y. Chen, H. He, and X.-G. Wen, Phys. Rev. B **95**, 235107 (2017).
[15] Y.-C. Wang, C. Fang, M. Cheng, Y. Qi, and Z. Y. Meng, arXiv:1701.01552.
[16] Y.-C. Wang, X.-F. Zhang, F. Pollmann, M. Cheng, and Z. Y. Meng, Phys. Rev. Lett. **121**, 057202 (2018).
[17] M. R. Norman, Rev. Mod. Phys. **88**, 041002 (2016).
[18] M. P. Shores, E. A. Nytko, B. M. Bartlett, and D. G. Nocera, J. Am. Chem. Soc. **127**, 13462 (2005).
[19] F. Bert, S. Nakamae, F. Ladieu, D. L′Hôte, P. Bonville, F. Duc, J.-C. Trombe, and P. Mendels, Phys. Rev. B **76**, 132411 (2007).
[20] P. Mendels, F. Bert, M. A. de Vries, A. Olariu, A. Harrison, F. Duc, J. C. Trombe, J. S. Lord, A. Amato, and C. Baines, Phys. Rev. Lett. **98**, 077204 (2007).
[21] J. S. Helton, K. Matan, M. P. Shores, E. A. Nytko, B. M. Bartlett, Y. Yoshida, Y. Takano, A. Suslov, Y. Qiu, J.-H. Chung, D. G. Nocera, and Y. S. Lee, Phys. Rev. Lett. **98**, 107204 (2007).
[22] T. H. Han, J. S. Helton, S. Chu, D. G. Nocera, J. A. Rodriguez-Rivera, C. Broholm, and Y. S. Lee, Nature (London) **492**, 406 (2012).
[23] M. Fu, T. Imai, T.-H. Han, and Y. S. Lee, Science **350**, 655 (2015).
[24] T.-H. Han, M. R. Norman, J.-J. Wen, J. A. Rodriguez-Rivera, J. S. Helton, C. Broholm, and Y. S. Lee, Phys. Rev. B **94**, 060409(R) (2016).
[25] R. H. Colman, A. Sinclair, and A. S. Wills, Chem. Mater. **23**, 1811 (2011).
[26] Z. Feng, Z. Li, X. Meng, W. Yi, Y. Wei, J. Zhang, Y.-C. Wang, W. Jiang, Z. Liu, S. Li, F. Liu, J. Luo, S. Li, G. qing Zheng, Z. Y. Meng, J.-W. Mei, and Y. Shi, Chin. Phys. Lett. **34**, 077502 (2017).
[27] X.-G. Wen, Chin. Phys. Lett. **34**, 090101 (2017).
[28] Y. Wei, Z. Feng, W. Lohstroh, C. d. Cruz, W. Yi, Z. F. Ding, J. Zhang, C. Tan, L. Shu, H.-Q. Wu, Y.-C. Wang, J. Luo, J.-W. Mei, Z. Y. Meng, Y. Shi, and S. Li, arXiv:1710.02991.
[29] Z. Feng, W. Yi, K. Zhu, Y. Wei, S. Miao, J. Ma, J. Luo, S. Li, Z. Y. Meng, and Y. Shi, Chin. Phys. Lett. **36**, 017502 (2019).
[30] R. H. Colman, A. Sinclair, and A. S. Wills, Chem. Mater. **20**, 6897 (2008).
[31] R. H. Colman, A. Sinclair, and A. S. Wills, Chem. Mater. **22**, 5774 (2010).
[32] B. Fåk, E. Kermarrec, L. Messio, B. Bernu, C. Lhuillier, F. Bert, P. Mendels, B. Koteswararao, F. Bouquet, J. Ollivier, A. D. Hillier, A. Amato, R. H. Colman, and A. S. Wills, Phys. Rev. Lett. **109**, 037208 (2012).
[33] E. Kermarrec, A. Zorko, F. Bert, R. H. Colman, B. Koteswararao, F. Bouquet, P. Bonville, A. Hillier, A. Amato, J. van Tol, A. Ozarowski, A. S. Wills, and P. Mendels, Phys. Rev. B **90**, 205103 (2014).
[34] D. Boldrin, B. Fåk, M. Enderle, S. Bieri, J. Ollivier, S. Rols, P. Manuel, and A. S. Wills, Phys. Rev. B **91**, 220408(R) (2015).
[35] P. Puphal, K. M. Zoch, J. Désor, M. Bolte, and C. Krellner, Phys. Rev. Mater. **2**, 063402 (2018).
[36] T.-H. Han, J. Singleton, and J. A. Schlueter, Phys. Rev. Lett. **113**, 227203 (2014).

[37] H. O. Jeschke, F. Salvat-Pujol, E. Gati, N. H. Hoang, B. Wolf, M. Lang, J. A. Schlueter, and R. Valentí, Phys. Rev. B **92**, 094417 (2015).
[38] T.-H. Han, E. D. Isaacs, J. A. Schlueter, and J. Singleton, Phys. Rev. B **93**, 214416 (2016).
[39] Z. Feng, Y. Wei, R. Liu, D. Yan, Y.-C. Wang, J. Luo, A. Senyshyn, C. d. Cruz, W. Yi, J.-W. Mei, Z. Y. Meng, Y. Shi, and S. Li, Phys. Rev. B **98**, 155127 (2018).
[40] K. Tustain, G. J. Nilsen, C. Ritter, I. da Silva, and L. Clark, Phys. Rev. Mater. **2**, 111405 (2018).
[41] Z. Liu, X. Zou, J.-W. Mei, and F. Liu, Phys. Rev. B **92**, 220102(R) (2015).
[42] D. Guterding, R. Valentí, and H. O. Jeschke, Phys. Rev. B **94**, 125136 (2016).
[43] R. W. Smaha, W. He, J. P. Sheckelton, J. Wen, and Y. S. Lee, J. Solid State Chem. **268**, 123 (2018).
[44] J. Rodriguez-Carvajal, Physica B **192**, 55 (1993).
[45] See Supplemental Material at http://link.aps.org/supplemental/10.1103/PhysRevB.100.155129 for the CIF file of the nuclear structure and the table of basis vectors.
[46] A. S. Wills, Physica B **276–278**, 680 (2000).
[47] A. S. Wills, Z Kristallogr. Suppl. **30**, 39 (2009).
[48] R. Chisnell, J. S. Helton, D. E. Freedman, D. K. Singh, R. I. Bewley, D. G. Nocera, and Y. S. Lee, Phys. Rev. Lett. **115**, 147201 (2015).